Journal of Microscopy, Vol. 237, Pt 1 2010, pp. 51–62
Received 21 May 2009; accepted 18 June 2009
doi: 10.1111/j.1365-2818.2009.03301.x

Time-lapse FRET microscopy using fluorescence anisotropy

D.R. MATTHEWS*,†, L.M. CARLIN*,†, E. OFO*, P.R. BARBER‡, B. VOJNOVIC‡, M. IRVING†, T. NG*,† & S.M. AMEER-BEG*,†

**Richard Dimbleby Department of Cancer Research, New Hunts House, Kings College London, Guy's Medical School Campus, SE1 1UL, U.K.*

†Randall Division of Cell and Molecular Biophysics, New Hunts House, Kings College London, Guy's Medical School Campus, SE1 1UL, U.K.

‡Gray Institute for Radiation Oncology & Biology, University of Oxford, Old Road Campus Research Building, Roosevelt Drive, Oxford OX3 7DQ, U.K.

Key words. Fluorescence anisotropy, FRET, high-content screening, microscopy, time lapse.

Summary

We present recent data on dynamic imaging of Rac1 activity in live T-cells. Förster resonance energy transfer between enhanced green and monomeric red fluorescent protein pairs which form part of a biosensor molecule provides a metric of this activity. Microscopy is performed using a multi-functional high-content screening instrument using fluorescence anisotropy to provide a means of monitoring protein–protein activity with high temporal resolution. Specifically, the response of T-cells upon interaction of a cell surface receptor with an antibody coated multi-well chamber was measured. We observed dynamic changes in the activity of the biosensor molecules with a time resolution that is difficult to achieve with traditional methodologies for observing Förster resonance energy transfer (fluorescence lifetime imaging using single photon counting or frequency domain techniques) and without spectral corrections that are normally required for intensity based methodologies.

Introduction

The move towards automated, high-speed fluorescence microscopy is prompted by the general realization that drug screening, for many disease models, requires a biological approach, as opposed to more biochemical methodologies. Activity observed in biochemical screening does not transfer to cell-based assays, a fact that is attributed to the complexity of the cellular system. The biochemical approach is one which can never reproduce the myriad, highly regulated intracellular signalling processes observed physiologically (Starkuviene, 2007). The move to cell-based assays addresses another important issue: that of toxicity. Again, the toxicology of drug compounds can only be examined in the context of cell-based assays. There appear to be two types of screening modalities for high-throughput or high-content, cell-based assays. The first type uses fluorescence intensity as the readout and uses mature technologies such as flow cytometry and plate readers. These have proved robust tools in a number of assays including the application of Förster resonance energy transfer (FRET) to monitor caspase activity and to observe the response of the intracellular signalling molecule cyclic adenosine monophosphate (González & Negulescu, 1998). The cell-based, high-throughput microscopy assays reported also use fluorescence as a read-out but have mainly been limited to the examination of morphological changes or translocation events upon application of small molecule drug compounds or small interfering RNAs (Neumann *et al.*, 2006). The growing number of publications and the availability of commercial systems (GE Healthcare, Waukesha, WI, U.S.A.; Molecular Devices, Sunnyvale, CA, U.S.A. and Blueshift Technologies, Sunnyvale, CA, U.S.A.) attest to the maturity of this approach. Although providing significant quantities of data, there are a number of drawbacks to screening based on morphological changes, the primary example being the issue of quantification. Firstly, there is the issue of quantification. Phenotypic assays rely on scoring systems and sophisticated pattern recognition software to provide the read-out from the assay, introducing an element of subjectivity. The morphology of the cell is often a down-stream indicator of drug activity and the subsequent deconvolution of the pathways involved in causing specific morphological changes is usually complicated. Often, there is a dynamic response in the assay which occurs due to a direct perturbation of a protein–protein interaction and

Correspondence to: Dr. Daniel Matthews. Tel: +44 2078 486221; fax: +44 2078 486220; e-mail: daniel.matthews@kcl.ac.uk

this simply cannot be observed by monitoring morphological responses.

The spatial resolution afforded by conventional, far-field microscopy is insufficient to resolve the specific inter-relationship between individual protein complexes occurring on the nanometre length scale. Measurement of the near-field localization of protein complexes may be achieved by the detection of FRET between protein-conjugated fluorophores (see, e.g. the review by Jares-Erijman & Jovin, 2003) and clearly it would be a major advantage to use this technique in an imaging modality for high-throughput/content screening. FRET is a non-radiative, dipole–dipole coupling process whereby energy from an excited donor fluorophore is transferred to an acceptor fluorophore in close proximity (Förster, 1948; Stryer, 1978). The dependence of the coupling efficiency varies with the inverse sixth power of the distance between donor and acceptor and is described in terms of the Förster radius (the distance at which the efficiency of energy transfer is 50%), typically of the order 1–10 nm. Excitation of the donor sensitizes emission from the acceptor that ordinarily would not occur. Because the process depletes the excited state population of the donor, FRET will both reduce the fluorescence intensity and the donor fluorescence lifetime. The advantage of using donor fluorescence lifetime to detect FRET is that the method is independent of fluorophore concentration, donor-acceptor stoichiometry and light path length and is therefore well suited to studies in intact cells (Ng *et al.*, 1999; Wouters & Bastiaens, 1999; Barber *et al.*, 2009). Combined with confocal or multiphoton microscopy techniques to examine the localization of effects in cellular compartments fluorescence lifetime imaging (FLIM) techniques to allow the determination of populations of interacting protein species on a point-by-point basis at each resolved voxel in the cell (Duncan *et al.*, 2004; Peter & Ameer-Beg, 2004; Parsons *et al.*, 2005; Peter *et al.*, 2005). Although FLIM remains the gold standard for measurement of FRET, particularly when issues such as interacting/non-interacting fractions of donors are considered, there is a need for faster metrics when dealing with dynamic events or when measurement time must be minimized; such constraints are routinely relevant to high-throughput screening and high-content screening. Fluorescence anisotropy is one such technique where measurement of the depolarization of sensitized acceptor emission has proven to be a robust, high dynamic range method for observing energy transfer (Piston *et al.*, 2008). This technique has been applied equally successfully in laser scanning and in wide-field modalities making it an excellent candidate for high-speed automated microscopy (Rizzo & Piston, 2005). To date, this method has been demonstrated using simple on-off caspase substrate biosensors which target the amino acid sequence Asp-Glu-Val_Asp (DEVD) and short defined-linker sequences which do not provide dynamic data with respect to protein interaction or activity. Many assays of protein interaction are either transient or cyclical, indicating a requirement for time-lapse imaging. A simple end-point assay is not enough to observed modified kinetics for an interaction especially when the protein of interest has many interaction partners. In this paper, we demonstrate the applicability of fluorescence anisotropy FRET imaging for dynamic high-content applications where protein interaction distances and/or populations may vary on relatively short timescales. These time-lapse dynamics serves as a surrogate for examining the dynamic range of a high content assay.

In this paper we discuss the in-house development of an automated high-content screening system which incorporates wide-field fluorescence anisotropy microscopy, which allows us to observe both donor and acceptor anisotropy in FRET assays to screen proteomic interactions. The assays of interest utilize Raichu biosensors comprising enhanced green fluorescent protein (eGFP) (Tsien, 1998) and monomeric red fluorescent protein (mRFP1) (Campbell *et al.*, 2002) separated by active sensing protein sub-units such that activation results in a conformational change of the biosensor, bringing the fluorescent proteins in close proximity and thereby increasing the FRET efficiency (Itoh *et al.*, 2005; Nakamura *et al.*, 2006). We have recently established these novel biological tools for imaging Rho GTPase (Cdc42 and Rac1) activity in T-cells by employing high-resolution, multiphoton FLIM (Makrogianneli *et al.*, 2009) and here we seek to apply this knowledge within the framework of high-content screening. The use of such biosensor probes for high-content screening applications is appealing, because there is 1:1 stoichiometry between donor and acceptor molecules. This property, taken in the context of fluorescence anisotropy, simplifies the data analysis because the FRET measurement obtained at each pixel will be dependent on the separation of the fluorescent proteins (as a measure of conformation) and not the relative acceptor:donor concentration. A number of end-point screening assays are currently under development in our laboratory using biosensor technology (e.g. using RNA interference [RNAi] to study the function of genes in cells (Fire *et al.*, 1998) and libraries of chemical compounds) but here we present data for Cdc42 and Rac1 activity in a live-cell imaging format. We will outline the well-known photo-physics of using acceptor anisotropy as a metric for energy transfer before describing the automated microscope developed for imaging this process. We examine the dynamic range and sensitivity of our system and show initial end-point assays performed in 96-well plates used to identify the baseline activity of the biosensor system. Time-course data are also described where we observe the dynamic behaviour of the localized activity of the protein complex.

Energy transfer and fluorescence anisotropy

Steady-state, and indeed time resolved, fluorescence anisotropy (or polarization) microscopy has proven to be a

highly sensitive technique, capable of identifying changes of the micro-environment of fluorescent molecules such as dipole orientation and viscosity (Levitt *et al.*, 2009). It has been shown to be a powerful technique for measurement of FRET for both protein homodimers (where FLIM alone cannot resolve interaction) (Gautier *et al.*, 2001) and, more recently, heterodimers (Rizzo & Piston, 2005).

In an isotropic solution fluorophores whose dipole moment is aligned to the electric field of the incoming polarized light will be selectively excited (a process collectively described as photoselection) (Dale & Eisinger, 1976; Dale *et al.*, 1979). The polarization retained by the emitted photons is determined by the amount of rotation the fluorophores undertake during the excited state lifetime. Fluorescence anisotropy provides a means for measuring the polarization that remains after excitation and therefore is traditionally used as a metric for fluorophore mobility and orientation. The Perrin equation (Lakowicz, 2006), given in Eq. (1) describes the relationship between anisotropy, r, the fundamental anisotropy (i.e. the anisotropy in the absence of rotational diffusion), r_0, the excited state lifetime, τ and the rotational correlation time, θ.

$$\frac{r_0}{r} = 1 + \frac{\tau}{\theta} \tag{1}$$

In FRET experiments, the propinquity of the donor and acceptor molecules means that molecules whose dipole moments are not aligned to the electric field of the excitation (those are not photoselected) can be excited. This means that polarized excitation of the donor molecules will result in depolarized emission from the acceptor molecules. In a homo-FRET experiment, energy transferred incoherently between spectrally identical fluorophores can be identified as a reduction in anisotropy rather than a reduction in donor lifetime. In a hetero-FRET experiment the energy transfer process results in a reduction in the donor lifetime and, as described by Eq. (1), an increase in donor anisotropy. This equation explicitly describes the relationship between the excited state lifetime (of the donor in a hetero-FRET experiment) and the rotational correlation time. If the rotational diffusion time is much greater than the excited state lifetime then the anisotropy tends towards the fundamental anisotropy. Additionally, if the excited state lifetime is reduced, as occurs in a hetero-FRET experiment then the anisotropy again increases toward the fundamental anisotropy. Conversely, and importantly for the technique described in this paper, the measured acceptor anisotropy is low because, under conditions where FRET occurs, the highly polarized nature of the donor and the unconstrained orientation of the acceptor molecule result in a strong depolarization of the acceptor molecule.

This effect is significant only when the rotational correlation time, θ, of the probes is slow compared to the rate of transfer, and the excited state lifetime. Fluorescent proteins are therefore excellent candidates for this technique. It has been shown that the anisotropy of eGFP in solution is of the order of 0.3 because it has a rotational correlation time in the region of 15–20 ns, compared to its excited state lifetime which is typically of the order of 2.2 ns. Large changes in anisotropy can occur for the sensitized emission for modest values of FRET efficiency resulting in an extremely sensitive, high dynamic range, measurement of the interaction between the fluorophores (Berberan-Santos & Valeur, 1991). In a high-content screen any drug, RNAi or inhibitor, or the interaction of the fluorescent proteins can therefore be identified in a straightforward and rapid manner by monitoring the behaviour of the acceptor anisotropy. This, of course, comes with a caveat: in assays where there is a significant difference between donor and acceptor concentrations additional controls are required to determine the concentration of each. Mattheyses *et al.* (2004) have demonstrated how this can be done in polarization microscopy.

Steady-state anisotropy can be determined as shown in Eq. (2):

$$r = \frac{I_{vv} - G\,I_{vh}}{I_{vv} + 2G\,I_{vh}} \tag{2}$$

Here r is the steady state anisotropy, I_{vv} and I_{vh} are the fluorescence emission intensities measured parallel and perpendicular, respectively, for the case where the linear polarization of the excitation is oriented vertically. The factor, G, is used to account for the different efficiencies for measurement of the two polarization directions within the system. In a microscope, where the excitation and detection paths are collinear the necessary correction is:

$$G = \sqrt{\frac{I_{vv}\,I_{hv}}{I_{hh}\,I_{vh}}} \tag{3}$$

In addition to background correction, and spectral bleed-through of green emission into the red channel, a number of other factors must be considered. The efficiency of the detection polarizers is extremely important for determining the anisotropy. In our system (described in detail below) we find a high efficiency in the green channel, but in the red channel there is a bleed through of the orthogonal polarization in each window of the order of 10%. We correct this bleed-through as follows (Siegel *et al.*, 2003):

$$I_{\mathrm{vvcorr}} = \frac{9\,I_{\mathrm{vvmeasured}} - I_{\mathrm{vhmeasured}}}{8} \tag{4}$$

$$I_{\mathrm{vhcorr}} = \frac{9\,I_{\mathrm{vhmeasured}} - I_{\mathrm{vvmeasured}}}{8} \tag{5}$$

Automated microscopy

The concept of automated microscopy, especially as employed in high content microscopy, is not a new one. The basic ethos

is labour reduction, enabling the skilled worker to engage in scientific research rather than the mundane task of operating a microscope. Of course, with the advent of high throughput and high content imaging, automation goes much further than this, the throughput being such that assays that could never have been considered can now be performed. An example of this being the concept of screening a library of drug compounds numbering hundreds of thousands. The high-throughput and high-content systems currently available commercially are based around intensity measurements; currently there has been just a single example reported in the literature of a high throughput system that incorporates a fluorescence lifetime element, which in this case was based on frequency domain measurements (Esposito *et al.*, 2007). Our approach to the field of high throughput and high content microscopy is essentially a modular one. All aspects of the platforms were developed in-house with commercially available components included wherever it was thought to be beneficial.

The automated system reported here allows the user to select between wide-field and laser scanning excitation for intensity-based and time-domain measurements, respectively. Here we concentrate on the wide-field component of the system and as such we direct the reader to reference (Matthews *et al.*, 2008) for more information about the FLIM component of the instrument. The output from a liquid light guide coupled mercury lamp (Intensilight, Nikon, Tokyo, Japan) is de-magnified and focused onto the pupil of an objective lens. The necessary linear polarized excitation is achieved by means of a polarizing beam-splitter and a half-wave plate. In this scheme the fluorescence emission from the sample of interest is detected by a polarization-resolved imager (Quadview, Photometrics, Tucson, AZ, U.S.A.), which splits the sample fluorescence emission with respect to both wavelength and polarization. A single charge-coupled device (CCD) (Orca-ER, Hamamatsu, Shizuoka, Japan) exposure therefore acquires four spatially identical images on different regions of the sensor. These sub-images are used to determine the fluorescence anisotropy of both donor and acceptor. The fluorophores of interest for this system are the enhanced green and monomeric red fluorescent proteins (eGFP and mRFP1, respectively) and as such the polarization resolved imager captures two orthogonal polarizations at wavelengths of 515 ± 30 nm and 630 ± 70 nm (filters obtained from Chroma Technologies, Rockingham, VT, U.S.A.). Of course, because this is essentially a wide-field microscope it can be utilized in more basic tasks such as monitoring expression levels, phenotyping and in long term time-lapse imaging (Agromayor *et al.*, 2009).

The instrument is equipped with a motorized stage (Märzhauser GmbH, Wetzler, Germany), a closed-loop objective focusing mount (Piezosystem Jena GmbH, Jena, Germany) with a 500 μm range of travel, and a motorized filter cube selector. All of these components are controlled using a I^2C bus via a single USB connection, and with an integrated modular software package developed at the Gray Institute for Radiation Oncology and Biology, Oxford University. The software provides the user with the ability to control every aspect of image acquisition including access to the Python scripting language for complete automation of an assay or screen. Currently, post-acquisition image processing is performed off-line using ImageJ and Matlab. The raw CCD images are saved in the image cytometry standard format that is capable of storing multi-dimensional data, in any numeric format along with image history or meta-data. Briefly, the original 1346×1024 pixel images acquired from the CCD camera and image splitter are deconstructed into four 694×495 pixel sub- images according to their wavelength and polarization channel from which the fluorescence anisotropy of each pixel can be determined as described above in Eqs (2)–(5). Image registration is implemented in a Matlab script using a field of point spread function fluorescent beads (with a nominal diameter of 170 nm) and a cross-correlation technique, details of which can be found in (Lu *et al.*, 2008). A mutual information joint entropy matrix is computed for the input images and maximized using Powel's direction set method (White, 1986). This is a rigid body image registration technique which calculates rotation and pixel offsets but not shear or scale. The routine takes a few minutes to run but needs only be calculated when the set-up of the microscope is changed; if the configuration of the image splitter or the objective is changed for example. The image registration parameters are saved in a configuration file for each microscope set-up and can be called by the user in a Matlab script used for batch processing of the large numbers of images generated during an experiment. Additionally the batch processing allows, at the discretion of the user, implementation of a Gaussian image filter and a masking routine to remove unwanted background pixels.

Calibration of the polarization resolved microscope

The maximum dynamic range achievable in acceptor FRET experiments is the contrast in anisotropy between the conditions of maximum interaction and zero interaction. That is, the lowest value of anisotropy is obtained when the FRET efficiency is highest, whereas a value of anisotropy approaching the intrinsic value for the fluorophore will be obtained when there is no interaction (of course, in a system where this means a total dissociation of the donor and acceptor, the intensity of the sensitized emission will drop to zero). This technique will also identify a change in the fraction of the interacting population. These two scenarios, respectively, represent the dynamic range and sensitivity of the measurement and the limits of these two have to be identified *a priori*. Our approach to this has been to measure the anisotropy of a fluorophore where the rotational correlation time can be controlled by the viscosity of the solvent in which it is dissolved. It is well known that rhodamine B is a highly mobile

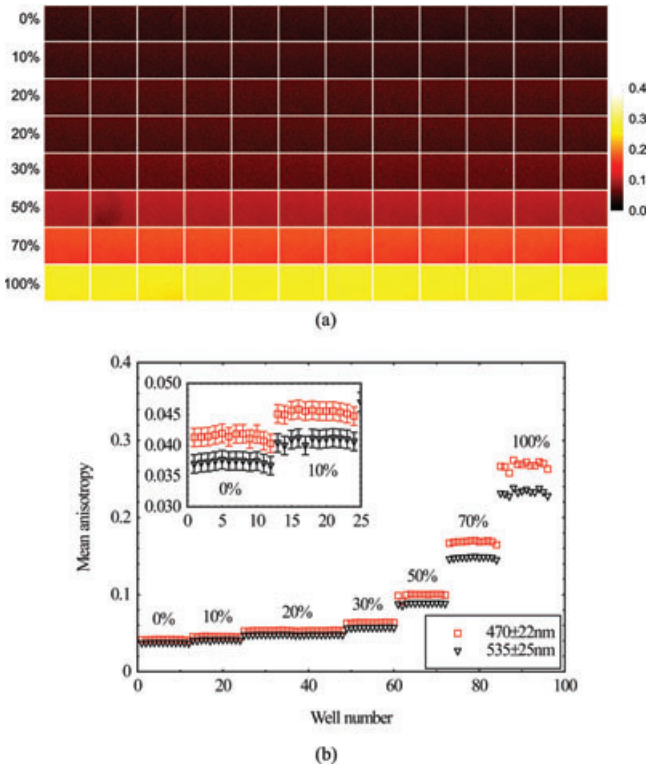

Fig. 1. (a) A montage of 96 anisotropy images of rhodamine B dissolved in water and glycerol. The amount of glycerol is given as a percentage, which varies within a column but is constant along the rows. (b) The mean value of the anisotropy for each image shown in (a). The red and black data markers are the measured values of anisotropy when the dye is excited at 535 ± 25 nm and 470 ± 22 nm, respectively.

molecule which is well described by the Perrin equation. Figure 1 shows a montage of anisotropy images of a 96-well plate with rhodamine B dispensed in each well. In each row of the plate the fluorophore is dissolved in water with different concentrations of glycerol (e.g. in the first row the rhodamine B is dissolved in water and in the last it is dissolved in glycerol). Figure 1(b) shows a plot of the mean anisotropy calculated for each well as a function of the well number with excitation wavelengths of 470 ± 22 nm and 535 ± 25 nm, and the same emission wavelength of 630 ± 70 nm. There a number of features evident in this graph. The rotational correlation time of the rhodamine B changes such that the anisotropy varies between 0.04 and 0.28, measured with a $20\times$ objective lens with a numerical aperture of 0.5. The measurement proves to be highly repeatable: there is very little well-to-well variation within the same row (i.e. when the solvent has the same viscosity). Our instrument also proves to be highly sensitive, identifying changes in anisotropy of $\sim$0.004: the inset of Fig. 1(b) shows that a change in concentration of glycerol of 10% is easily identified. In addition, the variation with excitation wavelength is easily observed (Chen & Bowman, 1965). The question remains as to the dynamic range and sensitivity that is required for acceptor FRET in a biosensor system.

Sensitivity and dynamic range are two issues to be resolved to produce reliable anisotropy images and both are dependent on signal-to-noise ratio (Lidke *et al.*, 2005). Ordinarily in a time-resolved FRET experiment the intensity of the sensitized emission is not a factor which is considered because the response of the donor is monitored upon interaction with an acceptor molecule. However when energy transfer processes are monitored using fluorescence anisotropy, the emissive properties of the acceptor molecule must be considered. Figure 2(a) shows a montage of images at different camera exposure levels with a scatter plot of the intensity of each pixel in the image as a function of the calculated anisotropy. This sequence of images of cancer cells expressing Cdc42-GFP demonstrates the robust nature of the anisotropy measurement to variations in the signal level versus the constant background signal. As the exposure time increases from 200 ms to 800 ms the full-width at half maximum is seen to decrease from 0.12 to 0.06 whereas the mean value of anisotropy in the image remains constant across the sequence. Figure 2(b) illustrates the effect of a fixed exposure time with varying the amount of frame averaging. As we increase the number of frames averaged in each acquisition from one to ten there is a marked improvement in the signal-to-noise level in the image as a whole. Increasing the number of averaged frames from one to ten improves the FHWM from 0.11 to 0.05. It is clear that both the exposure time and frame averaging need to be optimized to obtain an accurate value for the fluorescence anisotropy, and this is particularly true in a live cell experiment where photo-toxicity and photo-bleaching become important. These images demonstrate that, providing background and the G-factor are correctly accounted for, the technique can tolerate variations in signal-to-noise, and indeed the level of signal above the background, while still extracting a robust value for the fluorescence anisotropy.

Raichu biosensor molecules

Biosenors, termed 'Ras and interacting protein chimeric unit' (Raichu) probes, were constructed in our laboratory on the basis of the original design by Matsuda and co-workers (Itoh *et al.*, 2005). The Raichu probe consists of four components: the donor and acceptor fluorescent molecules; a GTPase and a GTPase binding region. Raichu probes (for Cdc42, Rac1 and RhoA) were modified in our laboratory to use eGFP and mRFP1 fluorescent proteins. Raichu-Rac and Raichu-Cdc42 use Rac and Cdc42 as their sensor regions and the CRIB domain of p21-activated kinase as the ligand region. As discussed earlier, the use of such biosensor probes for high-content screening applications is appealing, because there is 1:1 stoichiometry between donor and acceptor fluorescent proteins, making the data analysis more straightforward. Depending on the purpose of the screen, the protein pair can be chosen such that an external event (such as drug addition)

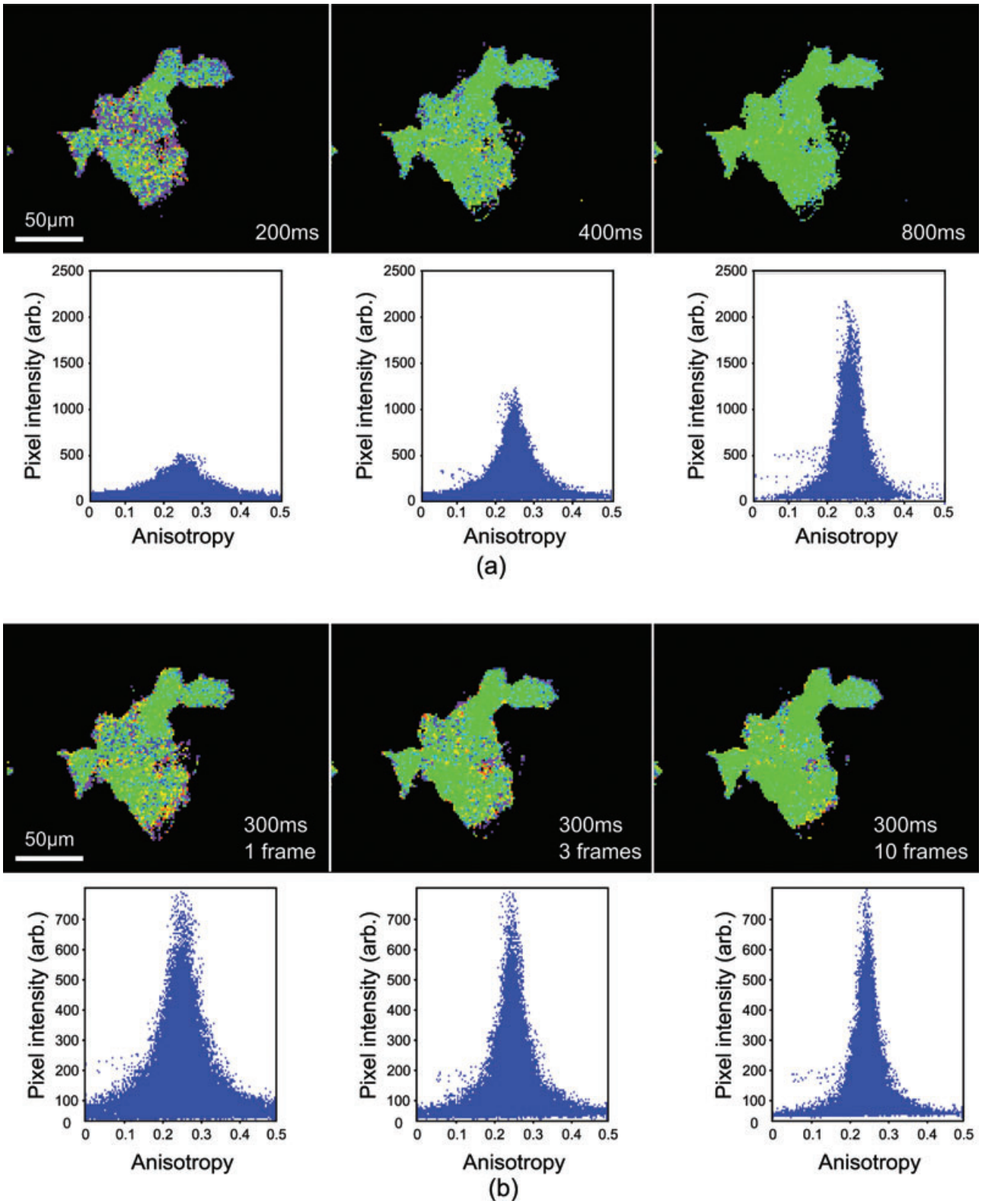

Fig. 2. (a) A series of images of A431 cancer cells expressing Cdc42-GFP where the camera exposure time is varied (with each camera exposure time given in the images). (b) The same A431 cells imaged with a camera exposure time of 300 ms. From left-to-right the number of frames that were averaged before calculating the anisotropy images was increased from 1 to 10.

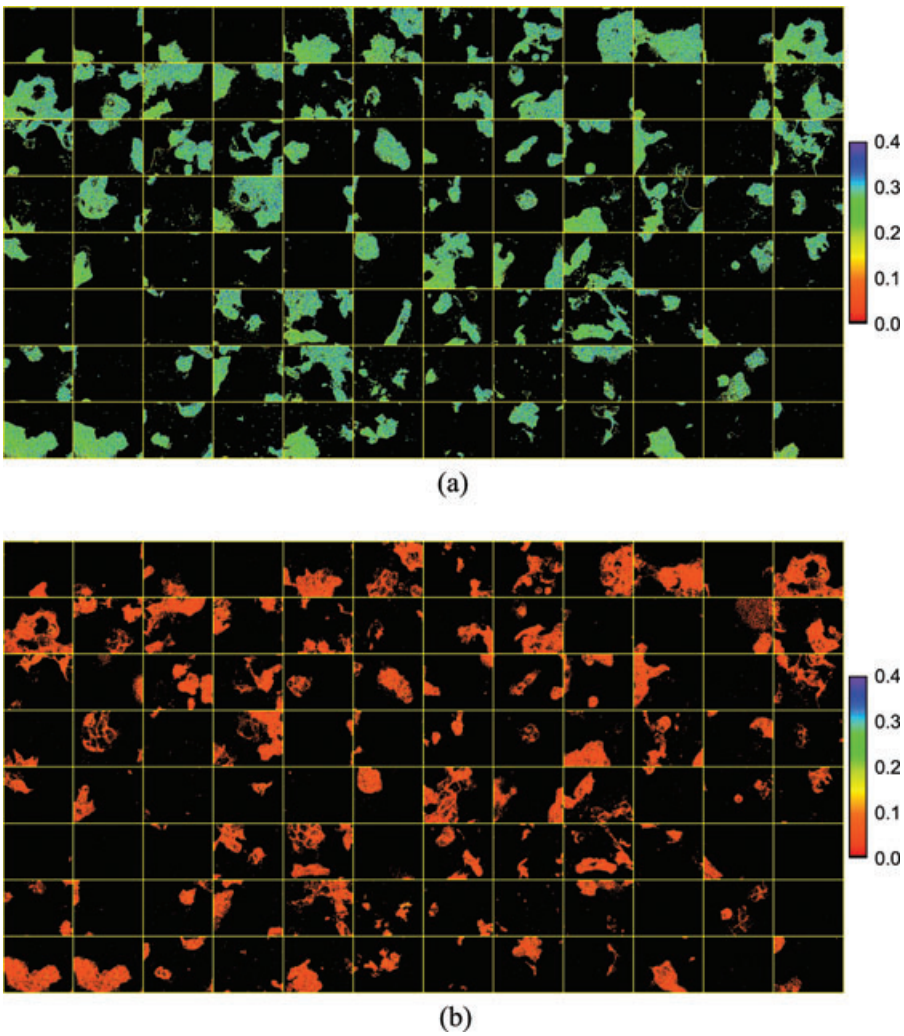

Fig. 3. (a) A montage of fluorescence anisotropy images of A431 cells expressing the Cdc42-Raichu biosensor when the RFP component is directly excited (at 535 ± 25 nm). This image clearly demonstrates the repeatability of the measurement: there is very little variation in mean anisotropy across the 96 wells of the plate displaying a mean value of around 0.3. (b) The same cells where the GFP component is excited and the sensitized RFP emission is measured. Again there is almost no variation in the mean fluorescence anisotropy (around 0.13) across the plate.

causes a gain or loss of association between proteins such that eGFP and mRFP1 are close enough to exchange energy non-radiatively.

Figure 3 shows images acquired from a 96-well plate within which we have cultured an epidermal human cancer cell line (A431) which is expressing the Raichu-Cdc42 biosensor. The two panels illustrate a number of features of the technique of anisotropy imaging using an automated microscope. Figure 3(a) shows the result of imaging the cells while directly exciting the RFP component of the biosensor; each image being one field of view of a 20× objective lens (200 × 150 μm field of view with the image splitter inserted). The image sequence was set-up by giving the microscope software the coordinates of seven wells in the plate, four of them the extreme corners, allowing the microscope software to interpolate the (x, y, z) coordinates of the rest of the multi-well plate using a polynomial fit for the z-coordinate, required due to the non-linear topography of the glass-bottom plate. Because the coordinates are generated automatically in this simple set-up it sometimes occurs that there are no cells within the field of view of the microscope, further software development will include a cell finding routine to further aid the user. The course value for the position of the image plane (z-coordinate) obtained from the polynomial fit to the plate topography is fine tuned during the unsupervised visitation of each of the 96 wells using a software auto-focus routine. Providing the signal-to-noise ratio is high enough each of the 96 wells can be imaged in two colour channels in around twenty minutes, with most of that time being taken up by the movement of the stage and the auto-focus routine. This general set-procedure has been designed such that it can be scaled up to much larger numbers of images.

In this proof-of-principle experiment each well is identical and as such each image appears as the same colour on this look-up-table, having an anisotropy value of around 0.25. The panel in Fig. 3(b) illustrates the activity of the biosensor. Here the GFP component is excited and we image the cells at the emission wavelength of the RFP: i.e. the anisotropy of the sensitized emission. The red colour of the images on this look-up-table indicates an anisotropy value of around 0.1. This lower value of anisotropy of the sensitized emission is due to the baseline activity of the biosensor. In fluorescence lifetime measurements this baseline activity typically indicates a FRET efficiency of the order of 10% (Matthews *et al.*, 2008).

This is in line with the calculation proposed by Jares-Erijman and Jovin (2003) for FRET efficiency using acceptor anisotropy. We prefer to report the anisotropy directly rather than conversion to FRET efficiency because this avoids certain assumptions regarding the system with respect to random distributions of acceptors (in our case, although we normally assume that the linkers between fluorophores and the biosensor modules are flexible enough to assume random distribution, this may not be true in both open and closed biosensor isoforms) and unknowns with respect to fluorophore extinction coefficients.

Rac1 activation in T-cells

High-content screening refers to the information content provided by an automated assay. In the majority of cases this term is used to describe an end-point assay where cells are dispensed into a multi-well plate, treated with a drug compound, for example and then fixed and imaged. Of course, imaging live cells is of paramount importance to cell biologists because time-lapse microscopy allows one to view the sequence of events that leads to a particular cell attaining a particular phenotype. Implementation of live-cell imaging in an automated high-throughput setting is an extremely challenging task. In addition to the technical issues encountered in high-throughput or high-content microscopy of fixed cells it is also necessary to track a particular cell or group of cells throughout the experiment and this presents a not-insignificant image processing challenge. Additionally if the live-cell experiment is to be scaled up to perform screening assays then compromise on time resolution must be made while still retaining the information content of the assay. It is clear that this would be extremely difficult to achieve with laser scanning techniques and so measurement of protein–protein interaction using FRET is better performed with a wide-field technique such as that described here.

Figure 4 shows both intensity and fluorescence anisotropy images from a live cell experiment performed using human Jurkat T-cells (obtained from ATCC) expressing the Rac1 variant of the Raichu biosensor and imaged with 0.75 numerical aperture 40× air objective lens (with a field of view of 100 × 75 μm). An incubation system, built into a 6-well plate with a coverglass bottom, and a lid which can be heated to avoid condensation of the media in the wells,

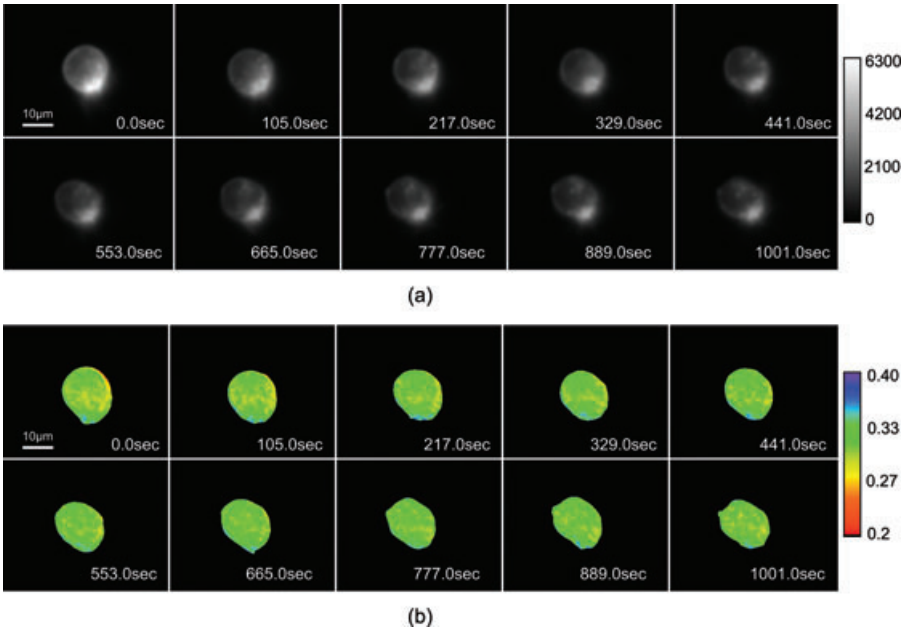

Fig. 4. (a) Selected frames from a live cell experiment examining the interaction of T-cells, expressing the Rac1 variant of the Raichu biosensor, with a CD3 antibody. The total time of the experiment was 30 min and images were captured every 5 s. (b) Fluorescence anisotropy calculated for each frame shown in (a). Here the RFP component of the biosensor is directly excited. The range of anisotropy values displayed is 0.2 to 0.4 in order provide maximum contrast in the images.

is used to keep the T-cells at 37°C, while also providing ports allowing exchange of gas and cell culture medium (WaferGen Smartsilde System (Labtech International Ltd, Ringmer, U.K.)). The inside of the glass has been coated with an activating anti-CD3 antibody (mAb UCHT1: Cancer Research UK London Research Institute monoclonal antibody service) and it is the effect of an antibody-mediated stimulation of the CD3 (part of the T-cell receptor complex) that we observe in the assay. We expect the interaction of the Jurkat cells with the antibody coated glass to cause a down-stream activation of the RhoGTPase Rac1, resulting in a change in the conformation of the biosensor, increasing its FRET efficiency. This particular interaction has been well documented, both using ratiometric techniques (Kurokawa *et al.*, 2004) and by time-domain lifetime measurements in a GFP-mRFP variation of the biosensor (Makrogianneli *et al.*, 2009).

Upon locating a cell of interest we acquire 1 s exposures with an interval of 5 s. The data in Fig. 4 show a selection of images which cover the total 30 min duration of a control experiment where we directly excite the RFP component of the biosensor molecules (see supplementary data for full sequence). Here the display look-up-table has been linearly adjusted to display values between 0.20 and 0.40 to provide maximum contrast in the images. As expected the mean fluorescence anisotropy from the directly excited protein has a value around 0.30 and the value does not vary throughout the time course, and its importance as a control is illustrated by the fact that there are no spatial variations in the anisotropy.

This can be contrasted with the dynamic variation in the activity of the sensitized emission, as illustrated in Fig. 5 where, for a different cell, we excite the GFP component of the biosensor molecules. As before we acquire 1 s exposures with an interval of 5 s and again we show a sequence of intensity images and the corresponding anisotropy images with a look-up-table that has been adjusted to display values between 0.08 and 0.24 (see supplementary data for the full sequence). This range was chosen again to provide maximum contrast in the images, something which cannot be achieved when the scale is made to be 0.0 to 0.4 (the maximum dynamic range available in a one-photon fluorescence anisotropy measurement). The spatial variation in the activity of the biosensor is very clear in these images as is the dynamic variation. It is evident that at the start of the experiment we chose a cell which is adhered to the glass plate. Over the course of the measurement the cell starts to detach from the glass surface and this correlates with a de-activation of the biosensor, an effect which can be clearly observed by the general increase in the blue colours in the images indicating localized increases in anisotropy. At the end of the experiment it seems that there is just one point of attachment: a region which has a low value of anisotropy and therefore high FRET efficiency throughout the entire time course. This of course is a fairly simple assay but it serves to illustrate that it is possible to monitor dynamic events in a FRET assay with good time resolution: this could not have been achieved with a time-domain technique, such as time-correlated single photon counting (TCSPC), due to the long acquisition times associated required with this technique. This

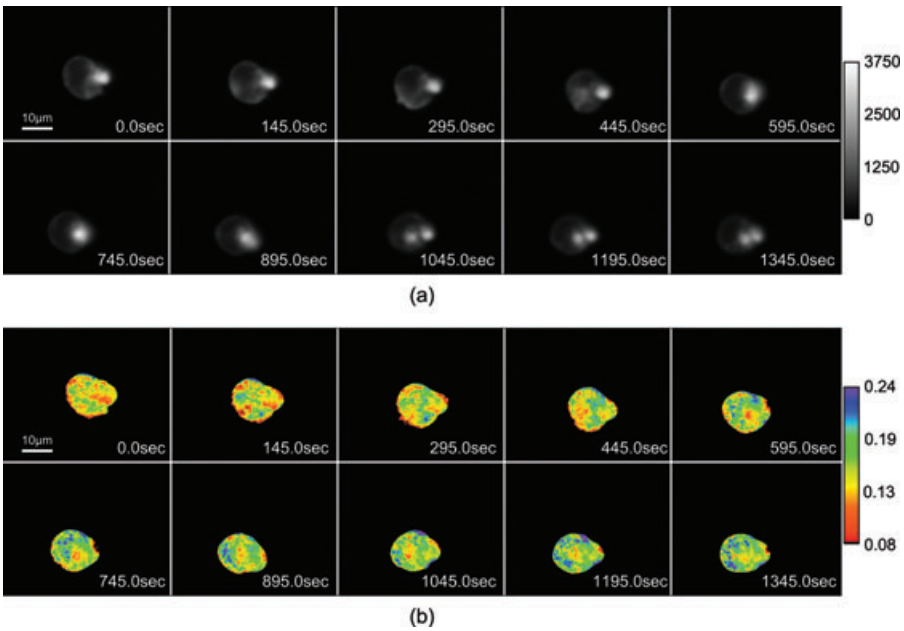

Fig. 5. (a) Intensity images from a different cell in the same experiment as that described in Fig. 4. (b) Fluorescence anisotropy images calculated for those frames displayed in (a). In this case it the anisotropy of the sensitized emission that is measured indicating the activity of the biosensor in response to the CD3 antibody. The spatial variation in anisotropy values indicates a variation in FRET efficiency and therefore biosensor activity.

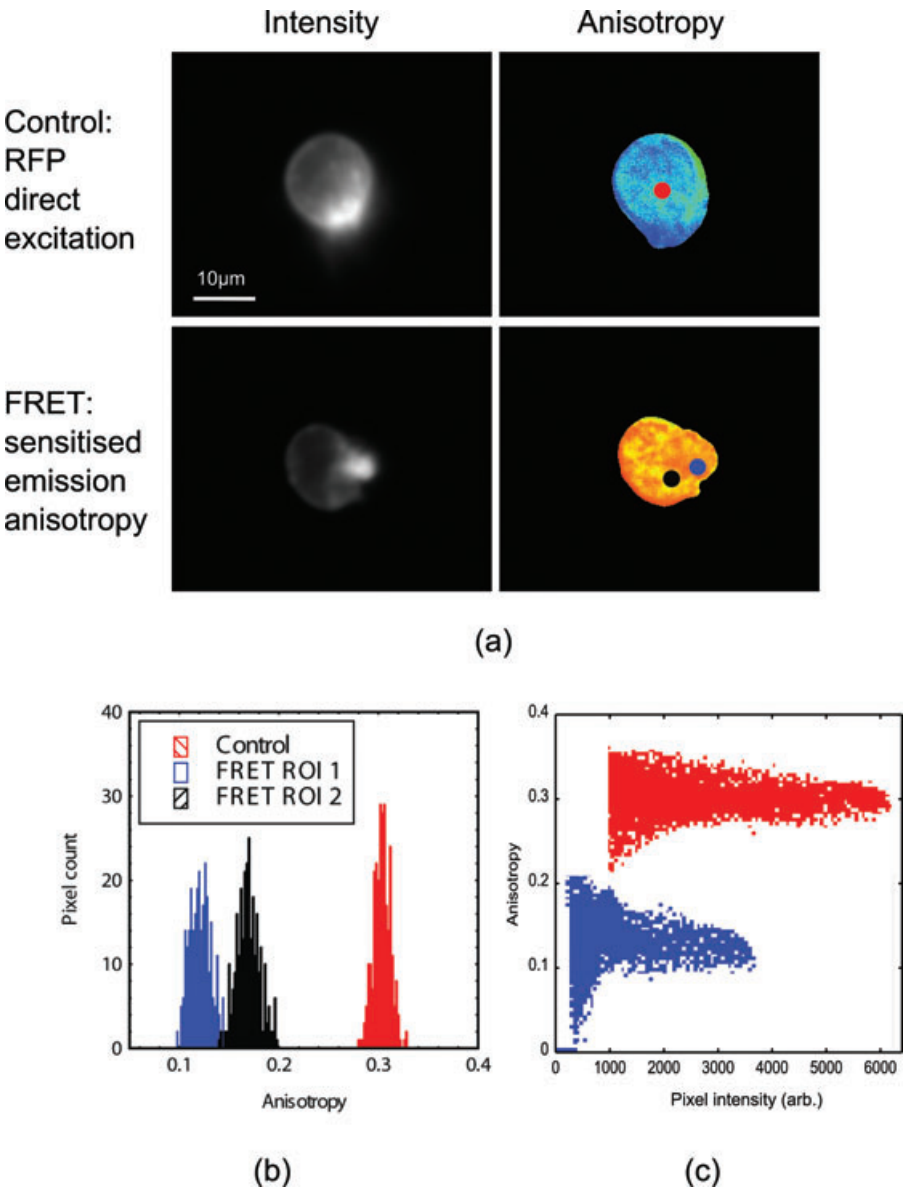

Fig. 6. (a) Intensity and fluorescence anisotropy images calculated for the first image in each of the time-lapse sequences discussed in Figs 4 and 5. (b) Shows histograms of pixel count versus anisotropy for the ROI marked on the anisotropy images of (a). The histograms are colour coded for their corresponding ROI in (a). (c) Scatter plots of anisotropy versus intensity for the entire image for each pair shown in (a).

clearly demonstrates that energy transfer causes the dynamic response of the sensitized acceptor emission giving a direct indication of the activation of the biosensor. It is also important to point out that in previous reports of this technique the FRET pair examined was totally dissociated during the assay providing the maximum dynamic range available; this was essentially a binary assay. Here we have demonstrated that acceptor anisotropy can be used to dynamically monitor FRET in a system where the biosensor undergoes conformational changes.

If we examine sub-cellular regions of interest (ROI) the magnitude of the spatial variations in anisotropy become clear. The first image in each sequence is shown in Fig. 6(a), where the anisotropy has been plotted on the same scale with a range of 0.0 to 0.4. Circular ROIs are marked on the images, from which a histogram of anisotropy, as a function of pixel count, is extracted (see Fig. 6b). The regions are coded such that the colour of this histogram data is that same as that of the ROI. In the control image, where the RFP is directly excited, the region shows anisotropy with a mean value of 0.3. When the pixel intensity is plotted as a function of anisotropy, as shown by the red markers in the graph plotted in Fig. 6(c), it is clear that the mean value of the image as a whole is again around 0.3. Figure 6(c) also demonstrates that there is no correlation

between pixel intensity and anisotropy in the image attesting to the fact that the signal-to-noise ratio is adequate to calculate a reliable value of the anisotropy.

The histograms plotted for the ROIs displayed illustrate the spatial variation in the anisotropy. Here the mean value varies between 0.12 and 0.17, an anisotropy difference which is much greater than that resolvable by the instrument (0.004). Again we plot the pixel intensity as a function of anisotropy of the whole image (the blue markers plotted in Fig. 6c). The mean value for the whole image is around 0.14 and the spatial variations manifest themselves as a wider standard deviation than that of the control experiment. This shows the importance of examining small ROI rather plotting the mean value of the anisotropy images over the whole time course: small spatial variations are not visible in the ensemble data. It is clear that more sophisticated software tools are required to track small ROIs throughout the time course.

Conclusions

Automated microscopy clearly has major benefits in terms of being a labour saving device but when combined with advanced quantitative imaging techniques can be a powerful tool in a number of different scenarios. Here we have demonstrated, using human cancer cell line (A431) the ability of an unsupervised microscope, combined with fluorescence anisotropy to perform quantitative imaging on large sample numbers. Live cell imaging has been performed examining the dynamic response of the Rac1 variation of the Raichu biosensor expressed in T-cells. This demonstrates the ability of the instrument to provide enough sensitivity and speed of data acquisition to measure the fast dynamic response of the T-cells following interaction of a surface receptor with an antibody coated multi-well chamber. It was clear that dynamic changes in the activity of the biosensor molecules could be tracked with a time resolution that could never be achieved in a TCSPC measurement, was done without the type of spectral bleed-through corrections that are normally required in ratiometric, steady-state measurements of FRET, and importantly, would be difficult with a manual microscope. Of course it is worth mentioning that other wide-field FLIM techniques exist which could be utilized to measure the dynamic response of such a biosensor but the implementation of these techniques, to provide a similar dynamic range, speed and sensitivity would be extremely demanding. This promising technique can be easily utilized, at low cost in comparison to wide-field FLIM techniques, in any assay where the FRET efficiency of the biosensor is a metric for a protein–protein interaction. Many further applications are currently being pursued in our laboratory including: screening of drug libraries, RNAi knock-down assays to perturb protein networks and further live cell assays which seek to quantify cycling of small Rho GTPases.

Acknowledgements

Daniel Matthews and Leo Carlin are supported by UK EPSRC grant 12 (EP/C546105/1). Enyinnaya Ofo is a recipient of both a Wellcome Trust Clinical Training Fellowship and the Dimbleby Cancer Care Award. Paul Barber and Borvoj Vojnovic are supported by Cancer Research UK (C133/A/1812). Simon Ameer-Beg and Tony Ng are supported by an endowment fund from Dimbleby Cancer Care to King's College London. The authors gratefully acknowledge the contribution of Robert Newman and John Prentice in constructing the microscope described in the text and the continued help of Glenn Pierce with software development.

References

Agromayor, M., Carlton, J.G., Phelan, J.P. *et al.* (2009) Essential role of hIST1 in cytokinesis. *Mol. Biol. Cell* **20**, 1374–1387.

Barber, P.R., Ameer-Beg, S.M., Gilbey, J., Carlin, L.M., Keppler, M., Ng, T.C. & Vojnovic, B. (2009) Multiphoton time-domain fluorescence lifetime imaging microscopy: practical application to proteinâ€"protein interactions using global analysis. *J. R. Soc. Interface* **6**, S93–S105.

Berberan-Santos, M.N. & Valeur, B. (1991) Fluorescence depolarization by electronic energy transfer in donor–acceptor pairs of like and unlike chromophores. *J. Chem. Phys.* **95**, 8048–8055.

Campbell, R.E., Tour, O., Palmer, A.E., Steinbach, P.A., Baird, G.S., Zacharias, D.A. & Tsien, R.Y. (2002) A monomeric red fluorescent protein. *Proc. Natl. Acad. Sci. U. S. A.* **99**, 7877–7882.

Chen, R.F. & Bowman, R.L. (1965) Fluorescence polarization: measurement with ultraviolet-polarizing filters in a spectrophotofluorometer. *Science* **147**, 729–732.

Dale, R.E. & Eisinger, J. (1976) Intramolecular energy transfer and molecular conformation. *Proc. Natl. Acad. Sci. U. S. A.* **73**, 271–273.

Dale, R.E., Eisinger, J. & Blumberg, W.E. (1979) The orientational freedom of molecular probes. The orientation factor in intramolecular energy transfer. *Biophys J.* **26**, 161–193.

Duncan, R.R. Bergmann, A., Cousin, M.A., Apps, D.K., Shipston, M.J. (2004) Multi-dimensional time-correlated single photon counting (TCSPC) fluorescence lifetime imaging microscopy (FLIM) to detect FRET in cells. *J. Microsc.* **215**, 1–12.

Esposito, A., Dohm, C.P., Bahr, M. & Wouters, F.S. (2007) Unsupervised fluorescence lifetime imaging microscopy for high content and high throughput screening. *Mol. Cell Proteomics* **6**, 1446–1454.

Fire, A., Xu, S., Montgomery, M.K., Kostas, S.A., Driver, S.E. & Mello, C.C. (1998) Potent and specific genetic interference by double-stranded RNA in Caenorhabditis elegans. *Nature* **391**, 806–811.

Förster (1948) Zwischenmolekulare Energiewanderung und Fluoreszenz. *Annalen der Physik* **437**, 55–75.

Gautier, I., Tramier, M., Durieux, C. *et al.* (2001) Homo-FRET microscopy in living cells to measure monomer-dimer transition of GFP-tagged proteins. *Biophys. J.* **80**, 3000–3008.

González, J.E. & Negulescu, P.A. (1998) Intracellular detection assays for high-throughput screening. *Curr. Opin. Biotechnol.* **9**, 624–631.

Itoh, R.E., Kurokawa, K., Fujioka, A., Sharma, A., Mayer, B.J. & Matsuda, M. (2005) A FRET-based probe for epidermal growth factor receptor bound non-covalently to a pair of synthetic amphipathic helixes. *Exp. Cell Res.* **307**, 142–152.

Jares-Erijman, E.A. & Jovin, T.M. (2003) FRET imaging. *Nat. Biotechnol.* **21**, 1387–1395.

Kurokawa, K., Itoh, R.E., Yoshizaki, H., Nakamura, Y.O.T. & Matsuda, M. (2004) Coactivation of Rac1 and Cdc42 at Lamellipodia and membrane ruffles induced by epidermal growth factor. *Mol. Biol. Cell* **15**, 1003–1010.

Lakowicz, J.R. (2006) *Principles of Fluorescence Spectroscopy*, Springer-Verlag, New York.

Levitt, J.A., Matthews, D.R., Ameer-Beg, S.M. & Suhling, K. (2009) Fluorescence lifetime and polarization-resolved imaging in cell biology. *Curr. Opin. Biotechnol.* **20**, 28–36.

Lidke, K.A., Rieger, B., Lidke, D.S. & Jovin, T.M. (2005) The role of photon statistics in fluorescence anisotropy imaging. *IEEE Trans. Image Process.* **14**, 1237–1245.

Lu, X., Zhang, S., Su, H. & Chen, Y. (2008) Mutual information-based multimodal image registration using a novel joint histogram estimation. *Comput. Med. Imaging Graph.* **32**, 202–209.

Makrogianneli, K., Carlin, L.M., Keppler, M.D. *et al.* (2009) Integrating receptor signal inputs that influence small Rho GTPase activation dynamics at the immunological synapse. *Mol. Cell. Biol.* 01008–01008.

Matthews, D.R., Ameer-Beg, S.M., Barber, P. *et al.* (2008) A high-content screening platform utilizing polarization anisotropy and FLIM microscopy. *Imaging, Manipulation, and Analysis of Biomolecules, Cells, and Tissues VI*, 1st edn. SPIE, San Jose, California.

Mattheyses, A.L., Hoppe, A.D. & Axelrod, D. (2004) Polarized fluorescence resonance energy transfer microscopy. *Biophys. J.* **87**, 2787–2797.

Nakamura, T., Kurokawa, K., Kiyokawa, E., Matsuda, M., William E. Balch, C.J.D. & Alan, H. (2006) Analysis of the spatiotemporal activation of Rho GTPases using Raichu probes. *Methods Enzymol.* **406**, 315–352.

Neumann, B., Held, M., Liebel, U., Erfle, H., Rogers, P., Pepperkok, R. & Ellenberg, J. (2006) High-throughput RNAi screening by time-lapse imaging of live human cells. *Nat. Meth.* **3**, 385–390.

Ng, T., Squire, A., Hansra, G. *et al.* (1999) Imaging protein kinase C activation in cells. *Science* **283**, 2085–2089.

Parsons, M., Monypenny, J., Ameer-Beg, S.M. *et al.* (2005) Spatially distinct binding of Cdc42 to PAK1 and N-WASP in breast carcinoma cells. *Mol. Cell. Biol.* **25**, 1680–1695.

Peter, M. & Ameer-Beg, S.M. (2004) Imaging molecular interactions by multiphoton FLIM. *Biol. Cell* **96**, 231–236.

Peter, M., Ameer-Beg, S.M., Hughes, M.K.Y. *et al.* (2005) Multiphoton-FLIM quantification of the EGFP-mRFP1 FRET pair for localization of membrane receptor-kinase interactions. **88**, 1224–1237.

Piston, D.W., Rizzo, M.A. & Kevin, F.S. (2008) FRET by fluorescence polarization microscopy. *Methods Cell Biol.* **85**, 415–430.

Rizzo, M.A. & Piston, D.W. (2005) High-contrast imaging of fluorescent protein FRET by fluorescence polarization microscopy. *Biophys. J.* **88**, L14–L16.

Siegel, J., Suhling, K., Leveque-Fort, S. *et al.* (2003) Wide-field time-resolved fluorescence anisotropy imaging (TR-FAIM): imaging the rotational mobility of a fluorophore. *Rev. Sci. Instrum.* **74**, 182–192.

Stryer, L. (1978) Fluorescence energy transfer as a spectroscopic ruler. *Annu. Rev. Biochem.* **47**, 819–846.

Tsien, R.Y. (1998) The green fluorescent protein. *Annu. Rev. Biochem.* **67**, 509–544.

Starkuviene, R.P. (2007) The potential of high-content high-throughput microscopy in drug discovery. *Br. J. Pharmacol.* **152**, 62–71.

White, S.D.M. (1986) Numerical recipes – the art of scientific computing – Presse,Wh, Flannery, Bp, Teukolsky, Sa, Vetterling, Wt. *Scientist* **1**, 23–23.

Wouters, F.S. & Bastiaens, P.I.H. (1999) Fluorescence lifetime imaging of receptor tyrosine kinase activity in cells. *Curr. Biol.* **9**, 1127.

Supporting Information

Additional Supporting Information may be found in the online version of this article:

Movie S1. A control live T-cell experiment where the fluorescence anisotropy of the mRFP1 component of the Raichu biosensor is excited directly at 535±35nm. Images were recorded with 1s exposures at an interval of 5s for a total duration of 30 minutes.

Movie S2. An image sequence from a live cell experiment examining the interaction of T-cells with a CD3 antibody. In this FRET experiment fluorescence anisotropy of sensitised mRFP1 is measured where images were recorded under the same conditions as the control experiment (1s camera exposures with a 5s interval for a total duration of 30 minutes). This sequence shows both the spatial and temporal variation of the Raichu biosensor activity.

Please note: Wiley-Blackwell are not responsible for the content or functionality of any supporting materials supplied by the authors. Any queries (other than missing material) should be directed to the corresponding author for the article.

